ISSN 0145-8752, Moscow University Geology Bulletin, 2011, Vol. 66, No. 5, pp. 323–330. © Allerton Press, Inc., 2011.
Original Russian Text © A.I. Koptev, A.V. Ershov, 2011, published in Vestnik Moskovskogo Universiteta. Geologiya, 2011, No. 5, pp. 25–32.

Thermal Thickness of the Earth's Lithosphere: a Numerical Model

A. I. Koptev and A. V. Ershov

Faculty of Geology, Moscow State University, Moscow, Russia

e-mail: koptev06@mail.ru; and@geol.msu.ru

Received February 15, 2011

Abstract—A technique is suggested and the thermal thickness of the lithosphere is calculated, as well as the temperature distribution in the lithosphere on the basis of data on topography, the age of the oceanic bottom, crustal composition and structure, gravity anomalies, and mean annual surface temperatures. The bottom of the lithosphere is determined as the 1300°C isotherm. The calculation resolution is 0.5° × 0.5°. All first-order tectonic structures, such as mid-ocean ridges and plume areas in oceans, continental rifts, cratons, and orogenic belts, are expressed in the computed thermal thickness. The comparative analysis of the thermal thickness of oceanic and continental lithosphere, lithosphere of cratons and young platforms, ancient and young orogens, remnant oceanic basins and adjacent continental areas can be used in geodynamical analysis of the corresponding regions.

Keywords: lithosphere, temperature distribution, thermal thickness, isostasy, numerical simulation, geodynamics.

DOI: 10.3103/S014587521105005X

INTRODUCTION

The lithosphere is understood as the relatively more competent outer shell of the hard Earth, which is located above the low-viscosity and more plastic asthenosphere. The term was first suggested by the American geologist J. Barell in 1914 (Barell, 1914). In the beginning, the lithosphere was identified with the Earth's crust; however, it was then ascertained that almost everywhere it includes the upper mantle from about several tens to several hundreds of kilometers in thickness. The position of the bottom of the lithosphere is determined by changes in the mechanical behavior of a medium: the bottom boundary of the lithosphere marks the transfer from the relatively hard and competent outer shell of the Earth (lithosphere) to the asthenosphere, which is characterized by higher plasticity due to the partly molten state of matter there. Thus, the lithosphere–asthenosphere boundary is reological in character, but not chemical–petrographical, like the crust–mantle boundary, where basic rocks of the lower crust change to ultrabasic mantle rocks.

However, changes in the reological properties of the mantle are not directly detectable in practice; therefore, the lithosphere bottom is more often detected by changes in the seismic wave travel velocity (the term "seismic lithosphere" is used in this case). To detect the approximate position of the lower boundary of the lithosphere in numerical calculations, it is often assumed that it passes along a certain preset isotherm (usually of about 1300°C, which is close to the solidus of mantle rocks). In such cases, one talks about thermal lithosphere and thermal thickness of the lithosphere.

At present, actual data have been obtained and published that allow valuable global quantitative estimation of the thermal thickness of the Earth's lithosphere. We used the topography (ETOPO5 relief numerical model by the National Geophysical Data Center, 1988), structural and matter analysis of the crustal composition (according to the data of CRUST 2.0 model (Bassin et al., 2000; Mooney at al., 1998)), gravity anomalies (EGM96 gravity model (Lemoine et al., 1988), age of oceanic bottom (Muller et al., 1997), and the distribution of mean annual surface temperatures as our data (Leemans et al., 1991; Lieth et al., 1972).

Based on this input data, the position of the lithosphere bottom and temperature distribution over it were computed. A global map of the computed thermal thickness of the Earth's lithosphere was obtained.

In contrast to previously published global models of the thermal thickness of the lithosphere (Artemieva and Mooney, 2001; Artemieva, 2006), we first adjusted the basic thermal model by means of corrections to isostatic compensation of the lithosphere and then performed calculations for the Earth's lithosphere as a whole, but not only for the continental lithosphere (Artemieva, 2006).

TECHNIQUE FOR COMPUTATION OF THE THERMAL THICKNESS OF THE LITHOSPHERE

We defined the thermal thickness of the lithosphere at each point of the Earth's surface as the difference

between the depth of the theoretical isotherm 1300°C and an absolute relief mark. The computation was performed on a grid with cells of 0.5 × 0.5°; the cell boundaries are oriented along parallels and meridians.

The isotherm position was determined from the model of thermal state of the lithosphere. The depth distribution of temperature differed for oceanic and continental lithosphere.

The depth (z) distribution of temperature $T(z)$ in the continental lithosphere was taken as steady-state and defined as

$$T(z) = T_0 + \int_{z_0}^{z} \frac{q(\zeta)}{k(\zeta)} d\zeta, \quad (1)$$

where T_0 is the surface temperature (the distribution over the computation grid was taken from (Leemans et al., 1991; Lieth et al., 1972)); z_0 is the absolute relief mark (according to the data from (National Geophysical Data Center, 1988)); $k(z)$ is the thermal conductivity coefficient; and $q(z)$ is the heat flow

$$q(z) = q_0 - \int_{z_0}^{z} A(\zeta) d\zeta, \quad (2)$$

$q_0 = q(z_0)$ is the surface heat flow. The specific volumentric heat production of lithospheric rocks was assumed to be exponentially decreasing with depth:

$$A(z) = A_0 \exp\left(-\frac{z}{H}\right), \quad (3)$$

where A_0 and H are the constants (3×10^{-6} W/s and 1×10^4 m, respectively) (Stein, 1995).

The depth distribution of the thermal conductivity coefficient was calculated in two different ways. In the first one, we used the equation

$$k(z) = A + \frac{B}{350 + T(z)}, \quad (4)$$

where the temperature T is measured in °C; the constants A and B for sediments are equal to 0.13 and 1073; for the upper and middle crust, 0.75 and 705; for lower crust, −1.18 and 474; for the mantle, 0.73 and 1293, respectively (Clauser and Huenges, 1995).

In another calculation approach, the distribution of the thermal conductivity coefficient in the upper and middle crust was defined according to (Germak and Rybach, 1982) as

$$k(z) = \frac{k_0}{1 + cT(z)}, \quad (5)$$

where k_0 is the thermal conductivity of corresponding rocks under surface conditions (which was taken equal to 3 W m^{-1} K^{-1}), and c is a constant that varies from 0 to 0.003°C (which was taken equal to 0.001°C). The thermal conductivity coefficient in sediments was considered constant and equal to 2.5 W m^{-1} K^{-1}; in the lower crust, 2 W m^{-1} K^{-1} (Seipold, 1992); and in the lithospheric mantle, 4 W m^{-1} K^{-1} (Schatz and Simmons, 1972; Scharmeli, 1979).

It turned out that the thermal thickness of the lithosphere weakly depends on the model of depth distribution of the thermal conductivity coefficient. Moreover, even if the coefficient is constant (3 W m^{-1} K^{-1}) throughout the lithosphere, the final calculation results deviated from the results obtained with the use of Eqs. (4) or (5) by no more than 10%. The results below have been obtained with the thermal conductivity coefficients calculated with the use of the second approach, i.e., Eq. (5).

Two approaches were used for calculation of the temperature distribution in the oceanic lithosphere. In the first case, the simplest linear temperature–depth dependence was used:

$$T(z) = T_0 + az. \quad (6)$$

In the second case, the temperature distribution in the oceanic lithosphere was calculated depending on its age within the model of a cooling half-space (Terkot and Shubert, 1985):

$$\frac{T(z) - T_0}{T_m - T_0} = \mathrm{erf}\left(\frac{z - z_0}{2\sqrt{\chi t}}\right), \quad (7)$$

where T_m is the temperature of the sublithospheric mantle (which was taken equal to 1444°C), χ is the thermal diffusivity (which was taken equal to 10^{-6} m^2/s) (Stein, 1995), erf is the error function, and t is the age of lithosphere. The age of oceanic bottom was taken from (Muller et al., 1997).

In this case, the main parameters that determine the thermal state of the lithosphere are the surface heat flow for the continental lithosphere and the age of the oceanic lithosphere. So the calculated temperature distribution is not accurate, because we do not know exactly the value of radioactive heat generation, coefficient of thermal conductivity of crustal rocks, thickness of crustal layers, and surface heat flow; in addition, the assumption of the stationarity of the thermal regime can be wrong for the continental lithosphere, or the model can fail to consider additional thermal factors, e.g., the hot-spot effect. Let us hereinafter call the model calculated only on the basis of the described thermal algorithms the basic model.

The basic model can be improved by using additional data. It is known that variations in temperatures of lithospheric rocks cause a change in their density, which, in its turn, affects the isostatic state of the lithosphere. In view of this, the model of isostatic compensation can be used for correction of the thermal model. According to the hypothesis of local isostasy for the lithosphere in local isostatic equilibrium, the weight of any two vertical lithospheric columns from the surface

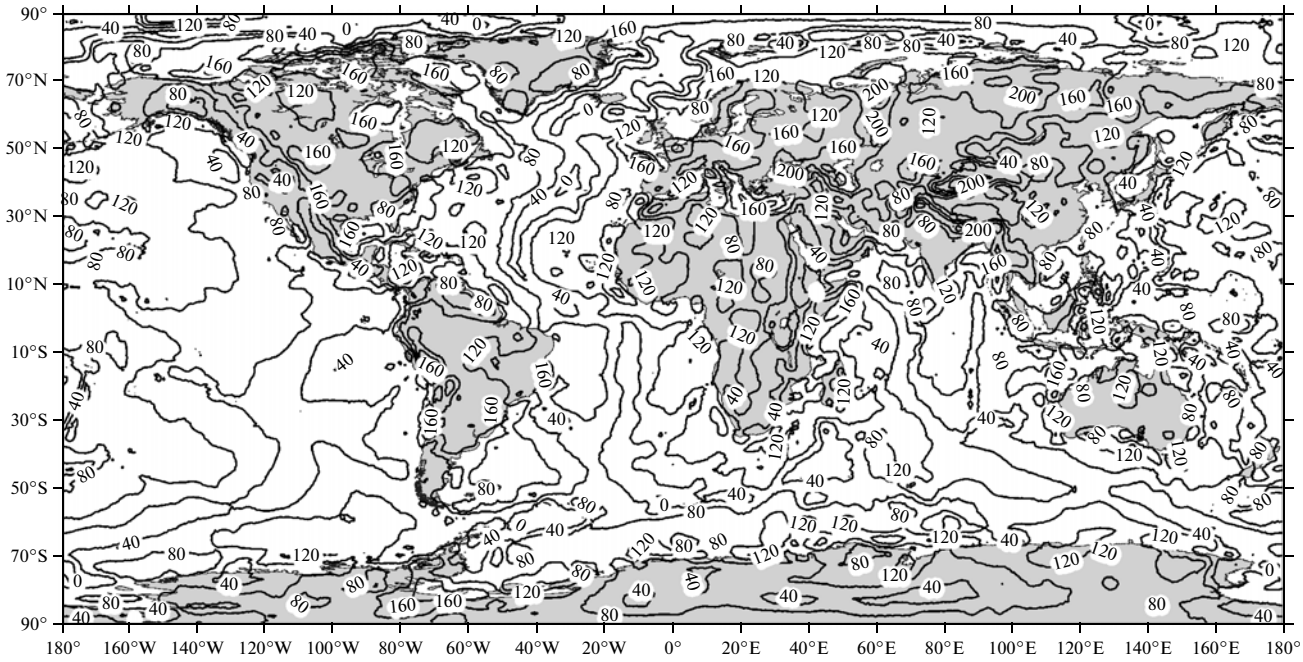

Fig. 1. Map of the calculated thickness of the lithosphere, in km.

to the depth of isostatic compensation should be equal:

$$\int_{z_0(x_1,y_1)}^{z_I} \rho(x_1, y_1, z)dz = \int_{z_0(x_2,y_2)}^{z_I} \rho(x_2, y_2, z)dz, \qquad (8)$$

where $z_0(x, y)$ is the absolute relief mark at the point with coordinates (x, y); z_I is the level of isostatic compensation; $\rho(x, y, z)$ is the density of lithosphere-composing rocks at the point with coordinates (x, y, z).

Corrections of the basic model due to the model of isostatic compensation were introduced as following. The surface heat flow q_0 in Eq. (2), the coefficient a in Eq. (6), and the age t in Eq. (7) were not considered as independent input parameters in calculations of the temperature distribution in the continental and oceanic lithosphere, respectively, but were calculated from the position of the 1300°C isotherm (bottom of the lithosphere), which was determined from the condition of local isostasy by Eq. (8).

The surface heat flow q_0 is expressed from Eqs. (1) and (2) as

$$q_0 = \frac{T(z_0 + H_L) - T_0 + \int_{z_0}^{z_0 + H_L} \frac{\left(\int_{z_0}^{\zeta} A(z)dz\right)}{k(\xi)} d\zeta}{\int_{z_0}^{z_0 + H_L} \frac{1}{k(z)} dz}. \qquad (9)$$

Thus, if we know the thickness of the lithosphere H_L, calculated within the model of isostatic equilibrium, we can calculate the surface heat flow. The coefficient a can be expressed via H_L from Eq. (6) as

$$a = \frac{T(z_0 + H_L) - T_0}{H_L}, \qquad (10)$$

and the lithosphere age, from Eq. (7) as

$$t = \frac{1}{\chi}\left(\frac{H_L}{2\mathrm{erf}^{-1}\left(\frac{T(z_0 + H_L) - T_0}{T_m - T_0}\right)}\right)^2, \qquad (11)$$

where erf^{-1} is a function that is inverse to the error function.

Thus, the isostatic model is related to the thermal one via the condition $z_I = z_{1300}$, where z_{1300} is the depth of the 1300°C isotherm.

If the temperature distribution in the oceanic lithosphere is calculated from the model of a cooling halfspace (7), then we can manage without isostatic corrections. In this case, calculation of the depth of the oceanic bottom from the model of isostatic compensation (8) (if the thickness of lithosphere and temperature and density distributions over it are known), and comparison of the calculation results with the real data can be a good criterion of correctness of the model.

Let us also note that we did not reveal any fundamental difference between the results of the models in which the temperature distribution in the oceanic lithosphere was calculated by Eqs. (6) and (7). The results shown in Fig. 1 and discussed in this work were

obtained with the use of a nonlinear temperature distribution over the oceanic lithosphere by Eq. (7).

Thus, to introduce the corrections in the basic model of lithosphere to the local isostasy effect, the thickness of lithosphere H_L should be calculated from Eq. (8). The thickness of ice cover, soft and hard sediments, and the upper, middle, and lower crystal crust were considered as known from the CRUST 2.0 data (Bassin et al., 2000; Mooney et al., 1998); therefore, the thickness of the mantle lithosphere was a calculated parameter in Eq. (8).

To calculate the density distribution over depth, the temperature dependence of the density of lithosphere-composed rocks ρ at a specified mineral composition at each cell of the computational grid was used:

$$\rho(T) = \rho(T_0)(1 - \alpha(T - T_0)), \quad (12)$$

where α is the volumetric thermal expansion of rocks (it was taken equal to 2.5×10^{-5}°C^{-1}) (Stein, 1995). The density at the surface temperature $\rho(T_0)$ for different crustal and upper mantle layers were also taken from the CRUST 2.0 model, while the temperature distribution in depth was calculated with the use of Eqs. (1–7).

The model of isostatic compensation used for correction of the basic thermal model can be refined due to accounting for data on free-air gravity anomalies in the calculations.

As is known (Terkot and Shubert, 1985), the anomalous gravity at each surface point can be expressed via the mass excess or deficit above this point by the Bouger formula

$$\Delta g = 2\pi G \int_0^h \rho(z)dz, \quad (13)$$

where Δg is the free-air gravity anomaly, G is the gravity constant (6.67×10^{-12} m^3 kg^{-1} s^{-2}). This formula is applicable the best to objects the thickness (h) of which is much smaller then the horizontal sizes.

Thus, if the hypothesis of local isostasy is completely fulfilled and the heights for any two laterally spaced lithosphere columns are equal (as is supposed in Eq. (8)), then the free-air gravity anomalies would be zero everywhere, which contradicts the real data. Therefore, the hypothesis of local isostasy should be corrected to the gravity anomalies, i.e., by accounting for Eq. (13), Eq. (8) should be extended to the equation

$$\int_{z_0(x_1,y_1)}^{z_I} \rho(x_1, y_1, z_1)dz - \int_{z_0(x_2,y_2)}^{z_I} \rho(x_2, y_2, z_2)dz = \frac{\Delta g_1 - \Delta g_2}{2\pi G}, \quad (14)$$

which shows that in the case of the absence of complete isostatic compensation, the difference in heights of spaced vertical lithosphere columns manifests in the difference in gravity anomalies above them.

For the calculations, the data on free-air gravity anomalies were taken in accordance with the EGM96 gravitational model (Lemoine et al., 1998).

When calculating the thickness of mantle lithosphere from Eqs. (8) and (14), the "standard" lithosphere column with a known thickness of the lithosphere, gravity anomaly, and density distribution should be specified for unambiguous definition of one of the parts of Eq. (8) in addition to the data on the structure of lithosphere, gravity anomalies, and temperature distribution over depth. As such a column, a column above a "standard" mid-ocean ridge has been chosen. It is characterized by following parameters: (1) the depth to the oceanic bottom is 3 km; (2) the total crust thickness is 6.5 km; (3) the mean crust density is 2850 kg/m^3; (4) the thickness of the mantle lithosphere is 0.85 km; (5) the density of the upper mantle is 3300 kg/m^3; and (6) the free-air gravity anomaly is 9.705×10^{-5} m/c^2.

The temperature distribution in the calculation algorithm is determined by the position of the bottom of the lithosphere, which, in its turn, depends on the temperature distribution. This uncertainty can be eliminated by the execution of a series of iterations, each of which includes the calculation of temperature distribution based on the position of the bottom of the lithosphere calculated at the previous iteration and calculation of a new corrected depth of the bottom of the lithosphere.

The necessity of selecting a value for the asthenosphere density contributes a significant uncertainty to the calculations. We defined it as the minimum of the difference between the upper mantle density minimum at the lithosphere bottom temperature (calculated by Eq. (12)) and a value of 3200 kg/m^3. Nonexceedance of the asthenosphere density above that of the lithosphere mantle is a necessary condition for the convergence of the above calculation iterations.

The surface heat flow was used as a basic input parameter for calculation of the temperature distribution in the lithosphere in the global thermal models of the lithosphere (Artemieva and Mooney, 2001; Artemieva, 2006). This resulted in certain difficulties connected with the inhomogeneous distribution of heat flow measurement points. Thus, the results of the interpolation of inhomogeneously distributed data of surface heat flow measurements were used for Precambrian craton regions (Artemieva and Mooney, 2001), while statistical processing, based on the derived correlation between the thermal thickness of the lithosphere and its age, was used for Phanerozoic continental regions (where reliable measurements of the surface heat flow are very scarce) (Artemieva, 2006). In this case, the condition of local isostasy was used only for estimation of the density of already calculated mantle part of the lithosphere and has no effect on the final position of the lithosphere bottom.

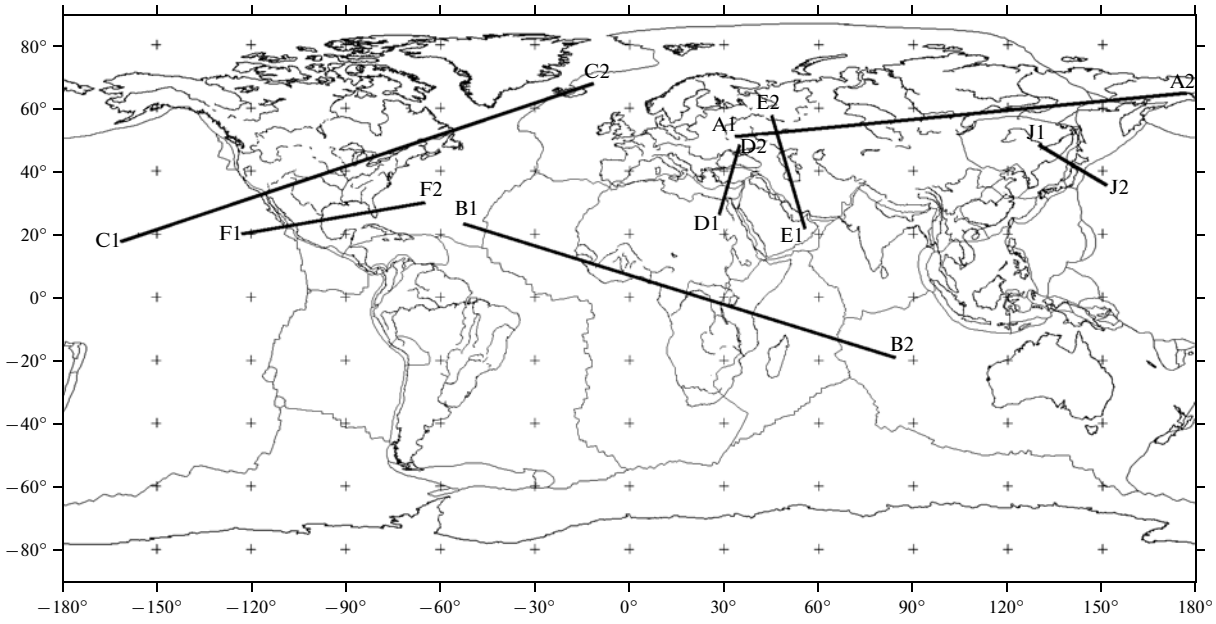

Fig. 2. Positions of section lines.

In addition to difficulties connected with the inhomogeneous distribution of measurement points, the use of surface thermal points as a calculation basis can cause some model uncertainty due to the probable effect of factors that are not connected with the depth thermal state of the crust on the surface heat flow, such as rapid sediment accumulation, underground water circulation, secular climate variations, significant variations in the thermal conductivity coefficient in the upper layers of sedimentary cover, and so on (e.g., (Smirnov, 1980)).

The isostatic corrections we used allowed weakening the effect of such factors as unstable heat flow and the uncertainly known value of the surface heat flow and thermal conductivity coefficient and parameters that determine the heat generation of rocks on the final result.

CALCULATION RESULTS

The calculated thermal thickness of the lithosphere is shown in Fig. 1; it reflects all the principal tectonic structures of the Earth. It significantly decreases down to zero values along the mid-ocean ridges, where, as is known, new oceanic lithosphere is generates. This peculiarity is seen in the B1–B2 section for the Middle Atlantic and Arabian–Indian spreading ridges (Figs. 2 and 3).

The age of oceanic lithosphere gradually increases with an increasing distance from mid-ocean ridges along with it thickness, which can attain 120–140 km at the continent–ocean interface. A natural increase in the thickness of lithosphere from the central part to periphery for Indian Ocean is shown in B1–B2 section, and for Atlantic Ocean, in B1–B2 and C1–C2 sections (Fig. 3).

Let us note that a significant decrease in the thickness of lithosphere is observed in plume regions in oceans (Hawaii and Azores, the Ninetieth Degree Ridge, Rio-Grande Swell, etc.) despite the above pattern. The Hawaii plume is well pronounced in the C1–C2 section; the Azores and Maskaren ridge plumes are evident in the B1–B2 section. The calculated thicknesses of the mantle lithosphere are negative for the Iceland plume, located at the mid-ocean ridge (the C1–C2 section). In the technical sense, this corresponds to non-fulfillment of the local isostasy condition, even in case of the complete absence of a mantle interlayer in the lithosphere; the physical sense of this phenomenon consists in the fact that the lithosphere in this area is extremely heated. In total, the thickness of the lithosphere does not exceed 150 km for the largest part of the oceans.

Within continents, minimum thicknesses of the lithosphere (from 0 to 40 km) are detected above continental rift systems (East African, Californian, Baikal, Myoma, Red Sea, etc.). Thus, North American structures (The Basin and Range province and Californian Ridge system) are clearly pronounced in a decrease in the thickness of the lithosphere in the C1–C2 and B1–B2 sections, respectively (Fig. 4); two branches (Western and Eastern) of the East African ridge system are well identified in the B1–B2 section.

The regions of craton development (East European, East Siberian, African, North American, etc.) are characterized by a thickness of lithosphere of 150–200 km (A1–A2, B1–B2, and C1–C2 sections). Younger orogenic belts in general are characterized by

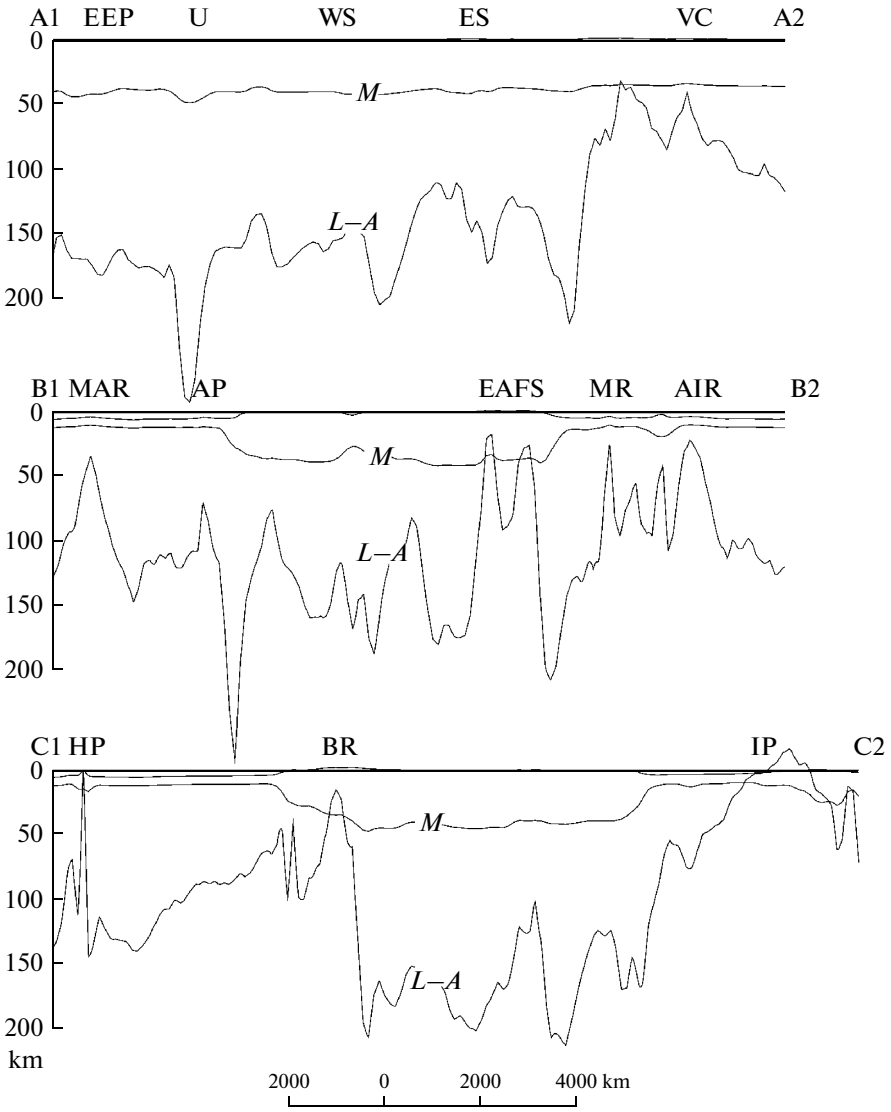

Fig. 3. A1–A2, B1–B2, and C1–C2 sections: *M* is the Mokhorovichich boundary, *L–A* is the lithosphere–asthenosphere interface; EEP is the East-European platform, WS is the West-Siberian platform; ES is the East-Siberian platform; VC is the Verchoyano-Chukotsk orogen, MAR is the Mid-Atlantic ridge, AP is the Azores plume, EAFS is the East-African rift system, MR is the Mascaren ridge, AIR is the Arabian–Indian ridge, HP is the Hawaii plume, BR is the Basin and Range province, IP is the Iceland plume.

a lower thickness of the lithosphere. For example, it is 120–130 km for the Caledonian Appalachian Mountains (the C1–C2 section) and 50–70 km for Mesozoic Verchoyano-Chukotsk orogen at about complete thinning of the mantle layer (A1–A2 section).

An interesting feature, shown in A1–A2 section, is the small difference between the lithosphere of the East-Siberian and East-European cratons and young Epi-Herzynian West-Siberian platform; the thickness of the lithosphere is about 100–150 km for these three cases. Let us note that these values agree with the data of deep-seismic sounding with using peaceful nuclear explosions, according to which layers with a decreasing velocity of seismic waves have been revealed at depths of 100–150 km (Pavlenkova, 2011).

An abnormal thickening of the lithosphere (up to 200–250 km) has been noted beneath the Herzynian orogenic belt of the Urals. Large values of the thickness of the mantle lithosphere beneath the Urals can be explained by the lighter crust in this region (according to CRUST 2.0 data).

We note the high values of the thickness of the lithosphere (200–220 km) for remnant oceanic basins with suboceanic crust. The Mediterranean and Black Sea basins are shown in the D1–D2 section; the thickened lithosphere of Southern and Northern Caspian basins are shown in the E1–E2 section, and the F1–F2 section shows thickening of the lithosphere beneath the Gulf of Mexico.

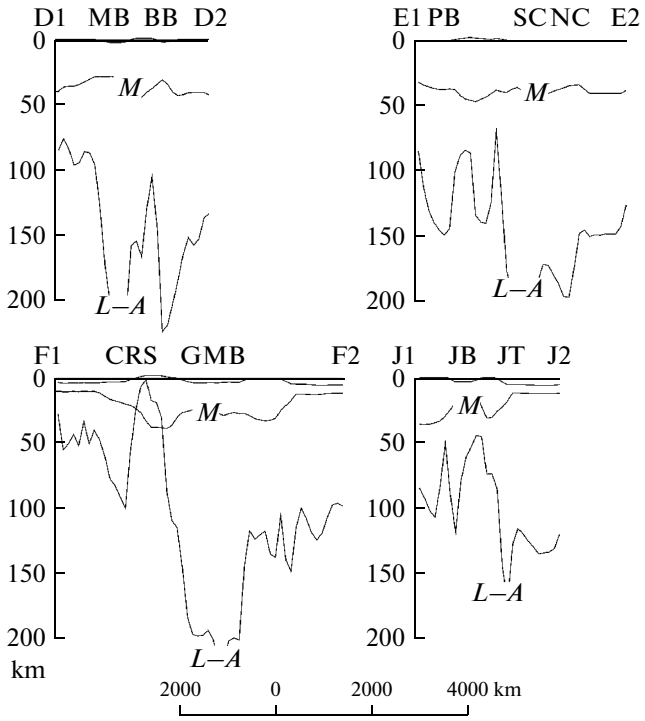

Fig. 4. D1–D2, E1–E2, F1–F2, and J1–J2sections: *M* is the Mokhorovichich boundary, *L–A* is the lithosphere–asthenosphere interface; MB is the Mediterranean basins, BB is the Black Sea basin, PB is the Persian Gulf basin, SC is the South-Caspian basin, NC is the North-Caspian basin, CRS is the Californian rift system, GMB is the basin of the Gulf of Mexico, JB is the Japan Sea basin, JT is the Japan Trench.

The character of the lithospheric thickness distribution in active continental margins is shown in the J1–J2 sections based on the example of the Japan subduction zone. Thickening of the lithosphere to 150 km, corresponding to a subducting oceanic slab, is observed immediately beneath the deep-sea basin. The thinning of the lithosphere to 50 km is detected beneath the ensialic crust of the Japan island arc, and thickening up to 100 km, in the back-arc Japan Sea basin.

Thus, the calculation results indicate that, on the one hand, the obtained thickness of the lithosphere agrees well with ideas about what it should be beneath such global structures as continental and oceanic rift systems, areas of within-plate oceanic magmatism, cratons, etc. The fact that the calculated thickness of the lithosphere takes expected values in places where it is known is evidence of the correctness of the accepted model. On the other hand, some features of the lithosphere thickness distribution, such as its significant increase beneath the Urals orogen, remnant basins of the Black, Mediterranean, and Caspian Seas, back-arc basins of the Japan Sea type, etc., are unobvious and can be a subject of further study and discussion.

Let us note that the presented results show generally lower values of lithosphere thickness beneath the continental regions as compared with earlier models (Artemieva and Mooney, 2001; Artemieva, 2006). A visible difference in the thickness of lithosphere beneath the continents of the Northern and Southern Hemispheres (underlined in (Artemieva and Mooney, 2001)) was not revealed in our model.

CONCLUSIONS

The thermal thickness of the Earth's lithosphere has been assessed on a calculation grid with cells $0.5° \times 0.5°$ in size. Data on topography, crustal structure and composition, gravity anomalies, age of oceanic bottom, and mean annual surface temperatures have been used in the calculations.

The bottom of the lithosphere has been determined from the position of the 1300°C isotherm, which corresponds to the solidus of the mantle crust. the temperature distribution in the continental lithosphere was considered as steady-state and was calculated based on the data on surface temperature and specific volumentric heat production in the crust and upper mantle. For the oceanic lithosphere, we used either the model of cooling half-space (age–temperature dependence of the distribution) or the simplest linear dependence of temperature on depth. To correct the thermal model, we used the model of local isostatic compensation.

The calculated thermal thickness of the lithosphere agrees well with the ideas about the thinning of the lithosphere beneath the mid-ocean ridges (Middle Atlantic, Arabian-Indian, Eastern Pacific, etc.) and plumes (Hawaii, Azores, Iceland, etc.) continental rift systems (East-African, Baikal, Californian, etc.). The thickness of the lithosphere beneath cratons (East-European, East-Siberian, North-American, etc.) is 150–200 km; it decreases to 50–70 km beneath younger orogenic belts (e.g., the Verchoyano–Chukotsk and Sikhote–Alin regions). Large values of the thickness of the lithosphere, which were obtained for the West Siberian platform (150 km), Urals orogen (220 km), trenches of Black, Mediterranean, and Caspian Seas (200 km), and back-arc Japan Sea basin (150 km) are of interest.

The data on the thermal thickness of the lithosphere can be used for the comparable geodynamic analysis of different tectonic structures and as input parameters for numerical calculations on the geodynamics of the lithosphere, e.g., in calculations of the global field of stresses and deformations of the lithosphere.

REFERENCES

1. Artemieva, I.M. and Mooney, W.D., Thermal Thickness and Evolution of Precambrian Lithosphere: A

Global Study, *J. Geophys. Res.,* 2001, vol. 106, no. B8, pp. 16387–16144.

2. Artemieva, I.M., Global 1° × 1° Thermal Model TC1 for the Continental Lithosphere: Implications for Lithosphere Secular Evolution, *Tectonophysics*, 2006, vol. 416, pp. 245–277.
3. Barrell, J., The Strength of the Earth's Crust, *Geology*, 1914, vol. 22, pp. 441–468.
4. Barrell, J., The Strength of the Earth's Crust, *Geology*, 1914, vol. 22, pp. 425–433.
5. Barrell, J., The Strength of the Earth's Crust, *Geology*, 1914, vol. 22, pp. 655–683.
6. Bassin, C., Laske, G., and Masters, G., The Current Limits of Resolution for Surface Wave Tomography in North America, *EOS Trans AGU*, 2000, vol. 81, p. 897.
7. Cermak, V. and Rybach, L., Thermal Conductivity and Specific Heat of Minerals and Rocks, *Landolt-Bornstein Numerical Data and Functional Relationships in Science and Technology*, New York: Springer, 1982, pp. 213–256.
8. Clauser, C. and Huenges, E., Thermal Conductivity of Rock and Mineral, *AGU Reference Shelf*, vol. 3: *Rock Physics & Phase Relations: A Handbook of Physical Constants*, Washington, DC: Amer. Geophys. Un., 1995, pp. 105–126.
9. Leemans, R. and Cramer, W., The IIASA Database for Mean Monthly Values of Temperature, Precipitation and Cloudiness on a Global Terrestrial Grid, *Res. Rep. RR-91-18*, Luxenburg: Instit. of Applied System Analysis, 1991, p. 61.
10. Lemoine, F.G., Kenyon, S.C., Factor, J.K., et al., The Development of the Joint NASA GSFC and NIMA Geopotential Model EGM96, *NASA/TP-1998-206861*, Greenbelt, Maryland: NASA Goddard Space Flight Center, July 1998.
11. Lieth, H., Modelling the Primary Productivity of the Earth. Nature and Resources, *UNESCO*, 1972, vol. 3, no. 2, pp. 5–10.
12. Muller, R.D., Roest, W.R., Royer, J.-Y., et al., Digital Isochrons of the Ocean Age, *J. Geophys. Res.*, 1997, vol. 102, no. B2, pp. 3211–3214.
13. Mooney, A., Laske, G., and Masters, G., Crust 5.1: a Global Crustal Model at 5 × 5 Degrees, *J. Geophys. Res.*, 1998, vol. 103, pp. 727–747.
14. National Geophysical Data Center. ETOPO-5 Bathymetry and Topography Data, *Data Announc. 88-MGG-02. NOAA*, Boulder, 1988.
15. Pavlenkova, N.I., Stroenie verkhnei mantii Sibirskikh platform po dannym yadernykh vzryvov, *Tez. Mezhdunar. Konf., Posvyashchennoi Pamyati V. E. Khaina "Sovremennoe Sostoyanie Nauk o Zemle"* (Abstracts of Intern. Conf. Devoted to the Memory of V. E. Khain "The Current State of Natural Sciences"), Moscow, 2011.
16. Scharmeli, G., Identification of Radio Active Thermal Conductivity in Olivine up to 25 Kbar and 1500 K, *Proc. of the 6th Air Apt. Conference,* New York: Plenum, 1979, pp. 60–74.
17. Schatz, J.F. and Simmons, G., Thermal Conductivity of Earth Minerals at High Temperatures, *J. Geophys. Res.*, 1972, vol. 77, pp. 6966–6983.
18. Stein, C.A., Heat Flow of the Earth, *AGU Reference Shelf*, vol. 1: *Global Earth Physics: A Handbook of Physical Constants*, Washington, DC: Amer. Geophys. Union, 1995.
19. Seipold, U., Depth Dependence of Thermal Transport Properties for Typical Crustal Rocks, *Phys. Earth Planet. Inter.*, 1992, vol. 69, pp. 299–303.
20. Smirnov, Ya.B., *Teplovoe pole territorii SSSR (poyasnitel'naya zapiska k kartam teplovogo potoka i glubinnykh temperatur v masshtabe 1 : 10000000)* (Thermal Field of the Territory of USSR: Memorandum to the Maps of Heat flow and Depth Temperatures in the 1 : 10000000 Scale), Moscow: GUPS, 1980.
21. Turcotte, D.L. and Schubert, G., *Geodynamics*, New York: Wiley, 1982.